Chapter IX. Physics of some edge plasma phenomena

In this chapter, we will discuss the physics of some macroscopic phenomena, which are distinctive for edge plasma. In particular, we will consider i) MARFE (Multifaceted Asymmetric Radiation From the Edge [1]) and poloidaly symmetric plasma detachment, ii) self-sustained divertor plasma oscillations and iii) divertor plasma detachment.

IX.1. MARFE and poloidaly symmetric plasma detachment.

Due to high plasma temperature in the core region of magnetic confinement devices, which ensures a high heat conductivity along the magnetic field lines, $\kappa_{||} \propto T^{5/2}$, plasma temperature can be considered constant on closed magnetic flux surfaces. However, in the edge region, where temperature and, therefore, plasma heat conduction are relatively low, strongly localized radiation losses can result in an inhomogeneous distribution of both plasma density and temperature over closed magnetic flux surfaces, even for the case where they have no direct contact with the materials of plasma-facing components. Then, obviously, plasma temperature will experience some depression in the region of high radiation losses. It is interesting, however, that the localization of enhanced radiation loss can be related to temperature depression itself. Indeed, recalling Fig. II.14 we can see that the cooling rate $L_{imp}(T_e)$ for low-Z (e.g. Carbon) impurity has non-monotonic dependence on electron temperature, and in the temperature range ~8-20 eV, $L_{imp}(T_e)$ for Carbon is increasing with decreasing electron temperature. This feature of $L_{imp}(T_e)$ provides positive feedback for the thermal plasma instability, which in the simplest case, can be obtained from the power balance equation where we neglect plasma dynamics and parallel heat conduction:

$$3n\frac{dT}{dt} = H - nn_{imp}L_{imp}(T)\,. \qquad \text{(IX.1)}$$

Here, for simplicity, we assume equal electron and ion temperatures, n and n_{imp} are plasma and impurity densities, and H is the plasma heating term, which is assumed to be constant. Then, assuming that temperature $T = T_0$ corresponds to the steady-state solution of Eq. (IX.1) and taking $T = T_0 + \tilde{T}$, where $\tilde{T} \propto \exp(\gamma t)$ describes a small departure from the equilibrium temperature, from Eq. (IX.1) we find the following expression for γ:

$$\gamma = -\frac{n_{imp}}{3}\frac{dL_{imp}(T)}{dT}\bigg|_{T=T_0}\,. \qquad \text{(IX.2)}$$

Expression (IX.2) predicts that the steady-state condition corresponding to $dL_{imp}(T)/dT < 0$ is unstable and can result in localized temperature drop accompanied by an increase of impurity radiation loss.

Such arguments were put forward in [1] to explain experimental observations of toroidally symmetric, rather compact in both poloidal and radial directions, and highly radiative region emerging at the inner side of the torus at high averaged plasma density in Alcator-C tokamak. In Fig. IX.1 one can see that the formation of MARFE at 120 ms is accompanied by a

strong increase of the radiation loss, as well as the H_α and CIII line radiation. In addition, in Fig. IX.2, one sees that the bolometer signal is locally increased in the MARFE region.

Predominant formation of MARFE at the inner side of the torus was explained in [1] by ballooning nature of cross-field heat transport from the core when the heat largely transported at the outer side of the torus (see Chapter VI for details) and arrives in the inner side due to parallel heat conduction.

However, in [2] and [3] it was pointed out that the simple model of plasma thermal instability described by Eq. (IX.1) that ignores plasma dynamics, misses an important feature related to the increase of plasma density in the region with reduced temperature. This effect is caused by plasma flow along the magnetic field lines, which is driven by the gradient of plasma pressure. Assuming that plasma flow entrains impurity and still neglecting parallel electron heat conduction, following [2] and [3] we find $\gamma \propto 2 - \mathrm{d}\ell\mathrm{n}\left(L_{\mathrm{imp}}(T)\right)/\mathrm{d}T\Big|_{T=T_0}$, which describes so-called radiative-condensation instability.

Due to plasma "condensation" in a low-temperature region, radiative-condensation instability can develop even for $\mathrm{d}L_{\mathrm{imp}}(T)/\mathrm{d}T > 0$. This instability plays an important role in many astrophysical and laboratory plasma phenomena (e.g. see [4] and the references therein).

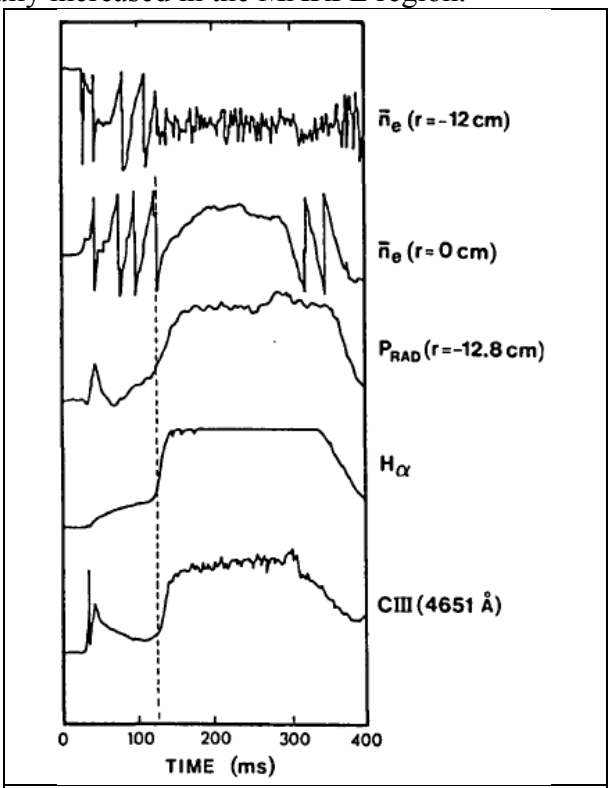

Fig. IX.1. Time traces from different diagnostics in Alcator-C tokamak. MARFE forms at 120 ms and is accompanied by enhanced: radiation loss at the inner side of the torus, H_α and CIII line radiations. Reproduced with permission from [1], © IAEA 1984.

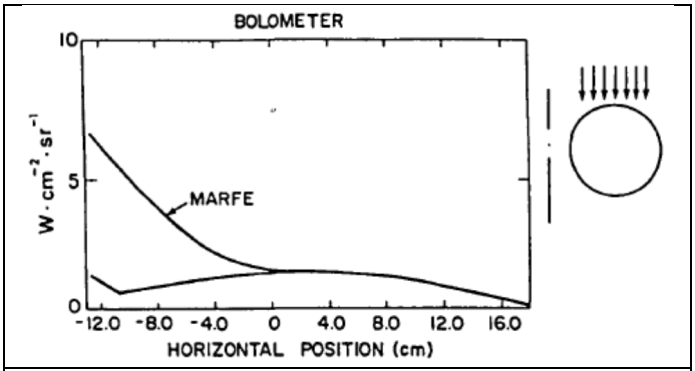

Fig. IX.2. Brightness profile as seen by the vertical bolometer view before and during MARFE. Reproduced with permission from [1], © IAEA 1984.

Although MARFE is observed at the inner side of the torus, poloidal localization of MARFE can oscillate in time (with the frequency ~ 100 Hz) around the midplane, whereas the localization of stationary MARFE (above or below the midplane) depends on the direction of the toroidal magnetic field [5]. The latter effect is attributed to the impact of drifts [6].

MARFE was observed on many tokamaks (see [7], [8], [9], [10], [11], [12], [5] and the references therein) as well on the stellarators LHD [13] and Wendelstein

7-X [14] at plasma density close to density limit [15].

Further studies of the MARFE phenomenon have shown that the physical picture of MARFE formation, which we outlined above and which is based on radiative-condensation instability, associated with impurity radiation is, at least, incomplete. Experimental data from TEXTOR and C-Mod tokamaks demonstrate that Hydrogen radiation loss and plasma recycling within the MARFE region can also play very important roles [16], [17]. Moreover, C-Mod data show that plasma temperature in the MARFE region falls below 1 eV whereas plasma density reaches $\sim 2\times10^{15}\mathrm{cm}^{-3}$, which stimulates very strong plasma recombination sink, which is close to plasma ionization source in the rest of the tokamak main chamber volume. As a result, the density of neutral Hydrogen in MARFE becomes so high that it traps about 95% of Ly_α and more than 50% of Ly_β radiation.

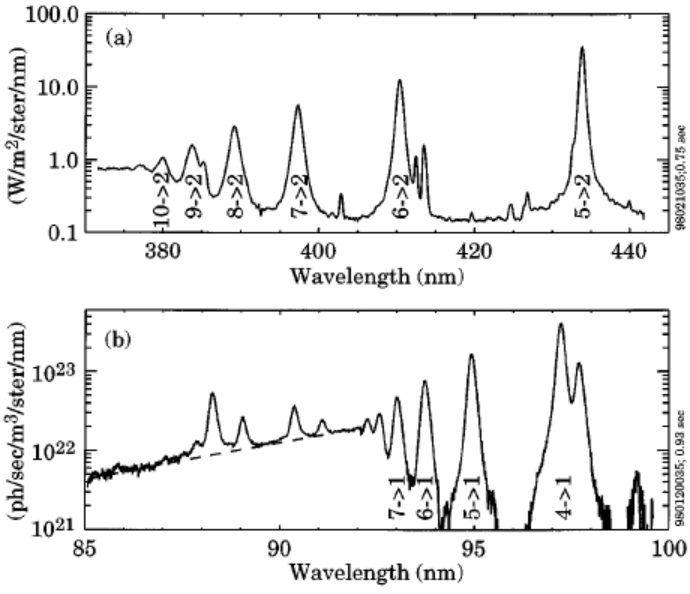

Fig. IX.3. Hydrogen radiation spectrum from MARFE in the visible (a) and VUV (b) lights. Reproduced with permission from [17], © American Physical Society 1998.

The spectrum of neutral Hydrogen radiation from MARFE in C-Mod tokamak, shown in Fig. IX.3, exhibits typical features of recombining plasma. Experimental data from Wendelstein 7-X stellarator also show the presence of plasma recombination in MARFE [14]. Theoretical analysis of an impact of plasma recombination on MARFE [18] shows that even though impurity radiation can be the initial trigger of MARFE formation, plasma recombination can facilitate MARFE development and, actually, determine deeply non-linear evolution of MARFE.

Finally, we note that the formation of MARFE is often accompanied by strong fluctuations of MARFE parameters and radiation from the MARFE region (e.g. see [17], [12], [5]). The latter can be associated with the poloidal motion of MARFE or relaxation oscillations, as it was found in numerical solutions of simplified plasma transport and impurity radiation equations describing the nonlinear stage of thermal instabilities and having characteristic frequency ~100

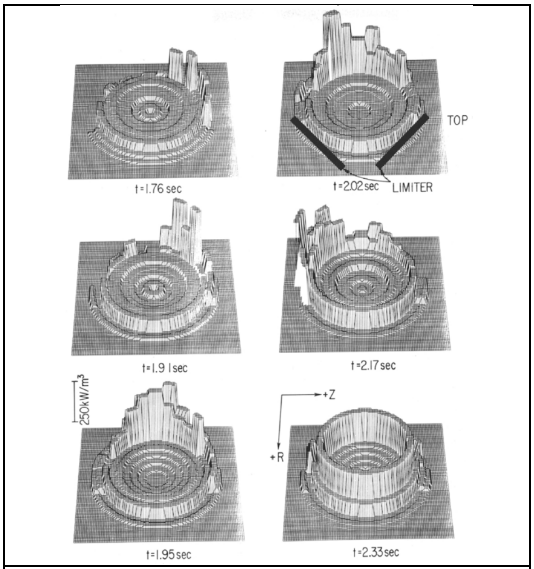

Fig. IX.4. Transition from MARFE to detached plasma in the TFTR tokamak. Reproduced with permission from [8], © Elsevier 1987.

Hz [2], [19], [20]. We note that some of the fluctuations, caused by the thermal force acting on the impurity [19], [20], have the form of self-sustained oscillations.

As we already mentioned, MARFE occurs at plasma densities close to the density limit. An increase of plasma density above the MARFE threshold often results in the transition of MARFE to detached plasma characterized by poloidally and toroidally symmetric highly radiative mantle (see Fig. IX.4).

In this regime, virtually all plasma heating power is dissipated by the radiation loss from the mantle (see Fig. IX.5) [21]. An excess of radiative power over ohmic heating in Fig. IX.5 is due to the calibration uncertainty.

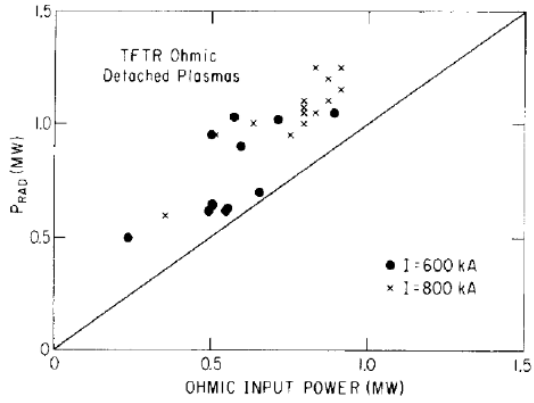

Fig. IX.5. Total radiative power compared to the ohmic heating power in the TFTR tokamak detached plasma. Reproduced with permission from [21], © Elsevier 1987.

Detached plasma was observed on many tokamaks in ohmic plasmas and with relatively low auxiliary heating (e.g. see [22], [8], [23], [24] and the review papers [25], [10]). Similar to the MARFE case, the formation of the radiative mantle can be accompanied by strong fluctuations of plasma parameters. For example, ~100% of the D_α signal fluctuations at the frequencies ~ 100 Hz were observed in the FT tokamak [22] (see Fig. IX.6), which shows a strong variation of the plasma recycling process. However, the physics of these fluctuations of plasma recycling is not known.

In addition, preliminary spectral measurements in detached plasma in C-Mod indicate that plasma recombination can be the major plasma sink.

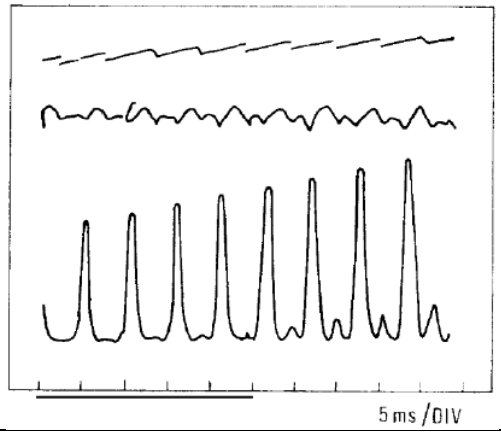

Fig. IX.6. From the top to bottom: sawtooth oscillations and time variation of loop voltage and the D_α signal from the detached plasma of the FT tokamak. Reproduced with permission from [22], © Elsevier 1982.

IX.2. Self-sustained divertor plasma oscillations.

As we have described in the previous section, such macroscopic phenomena as MARFE and detached plasma in limiter discharges are accompanied by the fluctuations of plasma parameters which look as self-sustained oscillations (e.g. see Fig. IX.6).

Actually, taking into account complexity and non-linearity of edge plasma processes, in particular, those where strong energy radiation losses play an important role, it is not surprising that edge plasma can exhibit regimes with self-sustained oscillations. Among other tokamak processes resulting in self-sustained oscillations, we can mention sawtooth oscillations and ELMs. However, these oscillations are closely related to MHD phenomena.

Somewhat similar to oscillations in MARFE and detached plasma self-sustained-like oscillations of plasma parameters were also found in the discharges with poloidal divertors (e.g.

see [26], [27]). Typical frequencies of these oscillations are about 100 Hz, which is close to the oscillation frequencies observed in MARFE and detached plasmas. Oscillations with similar frequencies were observed in detached regimes of the LHD stellarator [28]. As an example in Fig. IX.7 one can see such self-sustained oscillations found in L-mode discharges on JET tokamak [27], which were explained based on the theory developed in [29], [30].

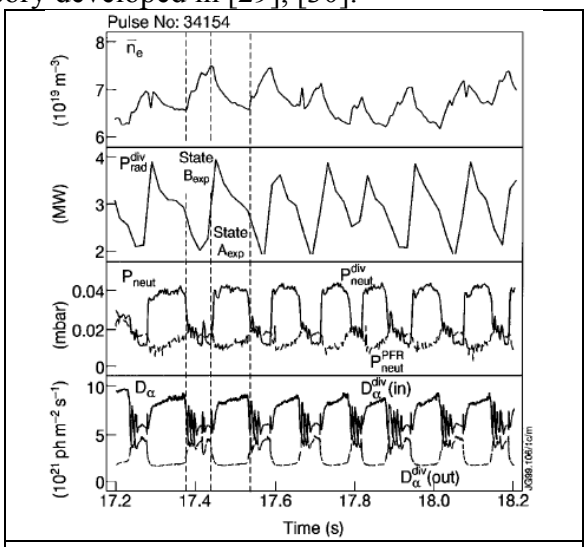

Fig. IX.7. Self-sustained oscillations of (from top to bottom) averaged density, divertor radiation, neutral density in inner divertor and private region, and inner/outer D_α emission observed in the JET tokamak. Reproduced with permission from [27], © American Physical Society 1999.

The main idea of [29], [30], which we also will use for the analysis of a tokamak divertor plasma detachment, is based on the properties of the high recycling regime of divertor operation. In these regimes, the neutral ionization mean-free path near the targets becomes very small, smaller than the corresponding width of the SOL. Therefore, the SOL can be considered as an ensemble of weakly interacting magnetic flux tubes filled with plasma and neutrals. The redistribution of plasma ions and neutrals along the magnetic field in the flux tube occurs rather quickly (characteristic time scales of ion and neutral redistribution are determined by sound speed and inverse ionization frequency respectively, which we will consider being much smaller than particle exchange time between different flux tubes. As a result, in a steady-state conditions total pressure (including contributions from both plasma and neutrals) in the flux tube, P_{ft}^{tot}, can be considered constant (except rather narrow region near the target where neutral friction with the target cannot be ignored) whereas the distributions of plasma and neutral gas parameters along the flux tube are determined by plasma and neutral transport processes and such input parameters as the heat flux propagating through the flux tube to the target, q_{ft}, and averaged density of neutrals and ions, N_{ft}^{tot}, in the flux tube. For simplicity, we ignore, for now, the effects of impurities.

We will be looking for the solution for the distributions of plasma and neutral gas parameters along the flux tube as well as for the plasma flux to the target. To elucidate the physics of the variation of plasma and neutral gas parameters, it would be useful to find dimensionless parameters governing the processes in the flux tube. However, first, we should determine the relevant dimensional parameters. Obviously, they include q_{ft}, N_{ft}^{tot} and the length of the flux tube L_{ft}. In addition, we need to allow for dimensional parameters describing collisional interactions of both the plasma and neutral particles. According to Chapter II, they are the electron charge, e, the Planck constant, $\hbar$, the electron (or ion) mass m (M), and the speed of light, c. However, it is more convenient to use dimensional parameters having clear physical meaning. Therefore, without any loss of generality, we substitute e, $\hbar$, and c with the Bohr radius, R_B, hydrogen ionization potential, I, and the lifetime of the first excited state of a

hydrogen atom, τ_{lt}, which is described by the Einstein coefficient from Chapter II. Thus, we have seven dimensional parameters (q_{ft}, N_{ft}^{tot}, L_{ft}, M (or m), R_B, I, and τ_{lt}), which completely determine all processes in the flux tube. Strictly speaking, the interactions of both the charged and neutral particles with material surface should provide some additional dimensional parameters (e.g. wall temperature, surface conditions, models describing hydrogen trapping, etc.). However, for simplicity, we assume that the interactions of both the charged and neutral particles with the material surface are described by some dimensionless energy and particle reflection coefficients which depend solely on the parameters of the species impinging on the surface. As a result, we still have only seven dimensional parameters defining the transport properties of plasma and neutrals within the flux tube and their interactions with the material surface. From these seven dimensional parameters, we can form four dimensionless ones.

We choose the dimensionless parameters that have simple physical interpretation:

$$\Pi_q = \frac{q_{ft}}{N_{ft}^{tot} I\sqrt{I/M}},\ \Pi_2 = R_B^2 N_{ft}^{tot} L_{ft},\ \Pi_3 = R_B^3 N_{ft}^{tot},\ \Pi_{step} = \tau_{lt} N_{ft}^{tot} R_B^2 \sqrt{I/m}. \quad \text{(IX.3)}$$

These parameters can be interpreted as follows: the parameter Π_q can be considered as the ratio of the available power q_{ft} to the power dissipated due to hydrogen recycling; the parameter Π_2 can be interpreted as the efficiency of neutral gas trapping (due to neutral ionization) within the domain of interest; Π_3 can be viewed as a factor determining the strength of multi-body processes (e.g. three-body recombination or charge screening), and Π_{step} can be interpreted as a factor controlling the effect of multi-step atomic physic processes (recall Chapter II).

As a result, the distributions of the plasma-neutral gas parameters (being expressed in the corresponding dimensionless form) along the flux tube are functions of the parameters (IX.3). For example, the electron temperature distribution $T_e(x)$ (where x is the coordinate along the flux tube) can be written as $T_e(x/L_{ft})/I = F_{Te}(x/L_{ft},\Pi_q,\Pi_2,\Pi_3,\Pi_{step})$, where $F_{Te}(x/L_{ft},\Pi_q,\Pi_2,\Pi_3,\Pi_{step})$ is some function. We notice that for a given L_{ft}, four dimensionless parameters can be collapsed to only two dimensionless parameters (e.g. Π_q and Π_3). Therefore, the plasma flux to the target, j_d, the plasma temperature at the target, T_d, and the pressure P_{ft}^{tot} can be written as

$$\frac{j_d}{N_{ft}^{tot}\sqrt{I/M}} = F_j(\Pi_q,\Pi_3), \qquad \frac{T_d}{I} = F_T(\Pi_q,\Pi_3), \qquad \frac{P_{ft}^{tot}}{N_{ft}^{tot} I} = F_P(\Pi_q,\Pi_3), \quad \text{(IX.4)}$$

where $F_j(\Pi_q,\Pi_3)$, $F_T(\Pi_q,\Pi_3)$, and $F_P(\Pi_q,\Pi_3)$ are some functions that cannot be determined from dimensionless analysis.

However, by adopting some simplifications we can estimate them. To do this, we start with deriving an expression that links the plasma temperature at the divertor target T_d with P_{ft}^{tot} and N_{ft}^{tot} (the latter we consider as the control parameter). From the energy balance equation in

the recycling region, allowing for both the flux of the plasma thermal energy to the target and energy dissipation due to hydrogen recycling, we have

$$q_{ft} = j_d \equiv n_d \sqrt{T_d / M} \left(\gamma T_d + E_{ion}^H \right), \qquad \text{(IX.5)}$$

where E_{ion}^H is the hydrogen "ionization cost" (recall Chapter II), which is determined solely by atomic physics represented by the dimensionless parameters Π_2, Π_3, and Π_{step}, as well as by the local (in the absence of the radiation trapping) dimensionless electron temperature and density. We assume that the ion temperature is lower than the electron one, $\gamma \sim 5 \div 8$ is the heat transmission coefficient (recall the results from Chapter IV). The first term in the brackets on the right-hand side describes the plasma thermal energy flux to the target, whereas the second one comes from energy dissipation due to hydrogen recycling, taking into account that in the high recycling regime, the plasma flux to the target is virtually equal to the neutral flux from the target.

For relatively high T_d, the neutral density at the target is lower than the ion density. This follows from the equality of the neutral and ion fluxes from and to the targets and the fact that the plasma flows along the magnetic field lines intercepting the target at a shallow angle. Therefore, the total momentum flux (pressure) is attributed to the plasma contribution, so we have $P_{ft}^{tot} = 2 n_d T_d$ (e.g. see [31]). And from Eq. (IX.5) we find [29], [30]:

$$P_{ft}^{tot} = \frac{2 q_{ft}}{\gamma T_d + E_{ion}^H} \sqrt{\frac{T_d}{M}} . \qquad \text{(IX.6)}$$

One can see from Eq. (IX.6) that the function $P_{ft}^{tot}(T_d)$ is non-monotonic. At large T_d, $P_{ft}^{tot}(T_d)$ increases with decreasing T_d, then reaches a maximum at $T_d = T_* \equiv E_{ion}^H / \gamma$:

$$\left(P_{ft}^{tot} \right)_{max} = q_{ft} \sqrt{\frac{M}{\gamma E_{ion}^H}} , \qquad \text{(IX.7)}$$

and then $P_{ft}^{tot}(T_d)$ decreases with increasing T_d.

Note that the ratio of the left- to the right-hand sides of Eq. (IX.5) for $T_d = T_*$ and $P_{ft}^{tot} = \left(P_{ft}^{tot} \right)_{max}$ gives us virtually parameter Π_1, which, as we discussed before, sets the limit, imposed by the available power, on the rate of plasma recycling.

To find the relation between N_{ft}^{tot} and T_d, we take into account the plasma outside the narrow, $<< L_{ft}$, recycling region, where there is no ionization source and the plasma flow is stagnant. Therefore, outside the recycling region, the only available mechanism to provide the energy flux q_{ft} is heat conduction. So we have $q_{ft} = \kappa_e(T) dT / d\ell$, where $\kappa_e(T) \propto T^{5/2}$ is the electron heat conductivity and ℓ is the coordinate along the magnetic field line (we take $\ell = 0$ at the target). Then we find the following expression for the electron temperature:

$T(\ell) = \left(T_d^{7/2} + q_{ft}\ell/\hat{\kappa}\right)^{2/7}$, where $\hat{\kappa} = (2/7)\kappa_e(T)T^{-5/2} = \text{const}$. As a result, assuming $T(L_{ft}) >> T_d$, using the expression for the plasma density $n(\ell) = P_{ft}^{tot}/T(\ell)$ and taking into account Eq. (IX.6), we find the following expression for the upstream plasma density $n_{up} \equiv n(L_{ft})$:

$$n_{up}(T_d) = P_{ft}^{tot}(T_d)\left(\frac{\hat{\kappa}}{q_{ft}L_{ft}}\right)^{2/7}. \qquad \text{(IX.8)}$$

Note that the expression virtually identical to Eq. (IX.7), (IX.8) was used in [32] as the justification for the SOL plasma density limit.

Similarly to the derivation of Eq. (IX.8) we find the dependence $N_{ft}^{tot}(T_d)$:

$$N_{ft}^{tot}(T_d) = L_{ft}^{-1}\int_0^{L_{ft}} n(\ell)\,d\ell \approx \frac{7}{5}P_{ft}^{tot}(T_d)\left(\frac{\hat{\kappa}}{q_{ft}L_{ft}}\right)^{2/7}, \qquad \text{(IX.9)}$$

and finally, we have

$$N_{ft}^{tot}(T_d) = \frac{2q_{ft}}{\gamma T_d + E_{ion}^H}\sqrt{\frac{T_d}{M}}\frac{7}{5}\left(\frac{\hat{\kappa}}{q_{ft}L_{ft}}\right)^{2/7}. \qquad \text{(IX.10)}$$

Examining the expression (IX.10) one finds that in accordance with our dimensionless analysis it can be re-written in terms of dimensionless parameters (IX.3) and the functions (IX.5).

As we see from Eq. (IX.6), (IX.8), (IX.9), the functions $n_{up}(T_d)$, $N_{ft}^{tot}(T_d)$, and $P_{ft}^{tot}(T_d)$ have a similar dependence on T_d, which seems to suggest that like P_{ft}^{tot}, both $n_{up}(T_d)$ and $N_{ft}^{tot}(T_d)$ have some maximum values, $n_{up}(T_d) \propto \left(N_{ft}^{tot}\right)_{max} \propto \left(q_{ft}\right)^{5/7}$. However, more detailed analysis and numerical simulations [29] show that the model we consider here is too crude to describe properly the recycling region for small T_d. In practice, the dependence $T_d(N_{ft}^{tot})$ for some cases can be described by an N-shaped curve shown schematically in Fig. IX.8. Moreover, as it often happens, some part of the N-shaped curve $T_d(N_{ft}^{tot})$ is unstable (see Fig. IX.8), and there is a bifurcation of $T_d(N_{ft}^{tot})$ dependence around $N_{ft}^{tot} \approx \left(N_{ft}^{tot}\right)_{max}$ [29], [30], [33]. With increasing N_{ft}^{tot}, there is an accumulation of neutrals in the vicinity of the target. Therefore the neutral pressure at the target, $P_d^{neut}(N_{ft}^{tot})$, increases with increasing N_{ft}^{tot} but it also exhibits the bifurcation at $N_{ft}^{tot} \approx \left(N_{ft}^{tot}\right)_{max}$ due to the transition from one stable branch of $T_d(N_{ft}^{tot})$ to the other one, see Fig. IX.8.

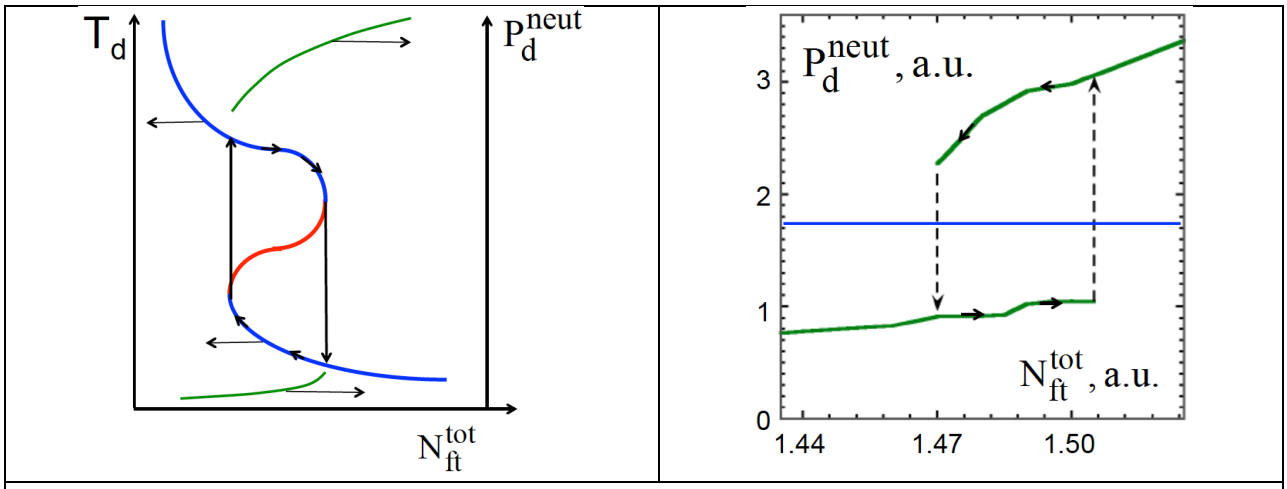

Fig. IX.8 (a) Schematic dependences of $T_d(N_{ft}^{tot})$ and $P_d^{neut}(N_{ft}^{tot})$. The unstable part of $T_d(N_{ft}^{tot})$ dependence is shown in red. (b) $P_d^{neut}(N_{ft}^{tot})$ dependence found from one-dimensional numerical modeling employing fluid plasma and Monte-Carlo neutral descriptions. The red line corresponds to the ambient neutral pressure $P_{d,amb}^{neut}$.

However, such a bifurcated solution exists only in the simplified one-dimensional model of the plasma within an isolated flux tube. When we allow for the effects of particle exchange between different flux tubes, we may see self-sustained oscillations of plasma parameters.

The physics of these oscillations can be illustrated with a very simple example. Assume that some flux tube is surrounded by plasma having the neutral pressure in the vicinity of the divertor target, $P_{d,amb}^{neut}$, such that it corresponds to the gap between the stable branches of $P_d^{neut}(N_{ft}^{tot})$ in the flux tube (see the red line in Fig. IX.8b). In this case, due to the neutral flow between the flux tube under consideration and the surrounding plasma (which can exceed the similar plasma flow caused by anomalous cross-field transport [30]), no steady-state equilibrium between the plasma within the flux tube and the ambiance becomes possible. As a result, self-sustained oscillations, corresponding to the limiting cycle indicated in Fig. IX.8 by arrows, develop.

In our simplified description of plasma parameters within the isolated magnetic flux tube, we ignored, for simplicity, the impact of impurity. However, the impurity radiation loss in the SOL plasma is ubiquitous. To incorporate the impurity radiation loss in the framework of plasma behavior within an isolated magnetic flux tube, we notice that the main energy losses caused by most of the impurities occur at plasma temperature higher than the temperature in the hydrogen recycling region (exceptions can be light elements having low ionization potential such as lithium).

Impurity radiation loss *per se* does not alter the plasma pressure, but just decreases the power available to sustain hydrogen recycling (we assume here that the fraction of impurity in overall plasma particle balance is small). As a result, the power flux reaching the hydrogen recycling region is $q_{recycl} = q_{ft} - q_{imp}$, where q_{ft} is the power flux propagating in the flux tube farther upstream and q_{imp} accounts for the reduction of this power due to impurity radiation.

Then, we find that the equations (IX.5)- (IX.7) still hold with the substitution of q_{recycl} instead of q_{ft}. If the impurity radiation region is localized at relatively small, $<< L_{ft}$, distance from the divertor target, then the expressions (IX.8), (IX.9) also hold. As a result, we find the following expression for $N_{ft}^{tot}(T_d)$:

$$N_{ft}^{tot}(T_d) = \frac{2\left(q_{ft} - q_{imp}\right)}{\gamma T_d + E_{ion}^H}\sqrt{\frac{T_d}{M}}\frac{7}{5}\left(\frac{\hat{\kappa}}{q_{ft}L_{ft}}\right)^{2/7}. \qquad \text{(IX.11)}$$

Thus, we conclude that $T_d(N_{ft}^{tot})$ can have an N-shape indicating bifurcation with impurity radiation loss. However, now the value of N_{ft}^{tot} corresponding to the bifurcation depends on q_{imp} and not only the neutral hydrogen pressure but also the neutral impurity pressure can bifurcate.

Then, the impurity exchange between the flux tube and ambiance will result in a change of q_{imp} and a shift of the N-shaped curve $T_d(N_{ft}^{tot})$ along the N_{ft}^{tot} axis. A mismatch of the ambient neutral impurity pressure and the neutral impurity pressure corresponding to the stable branches will also result in self-sustained oscillations of plasma parameters. An example of such impurity-driven oscillations is shown in Fig. IX.9.

Note that careful numerical analysis performed in [34] confirmed that self-sustained oscillations driven by impurity radiation, which are observed in numerical simulations of ITER divertor plasmas, are not related to computational issues.

IX.3. Divertor plasma detachment.

In the first subsection, we already discussed detached plasma regimes. However, that was toroidally and poloidaly symmetric detachment of plasma situated on "closed" magnetic flux surfaces, where plasma interaction with material surfaces (e.g. limiters, main chamber wall) is driven largely by cross-field transport. Here we consider detachment of plasma situated in the divertor volume on "open" magnetic field lines intersecting the divertor targets. In this case, plasma interaction with the divertor target material is mainly driven by plasma transport along the magnetic field lines.

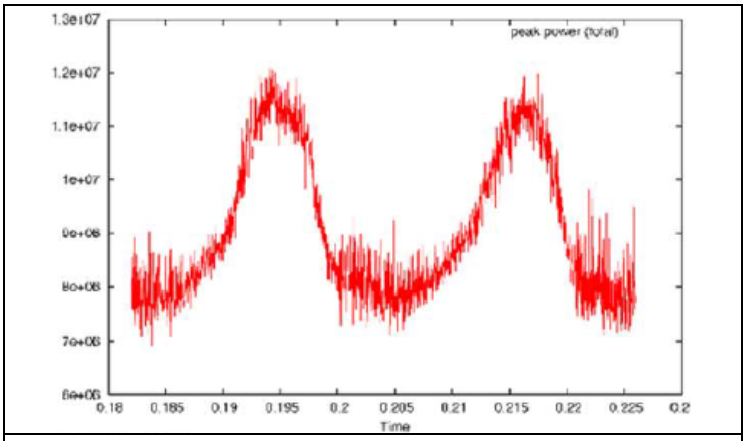

Fig. IX.9. Impurity (neon) driven self-sustained oscillations of the heat load on the outer divertor target found in 2D modeling of ITER. Reproduced with permission from [33], © IOP Publishing 2019.

There are different ways to define the "depth" of divertor plasma detachment. Here we will call the divertor plasma detached when there is a rollover of the ion flux to the divertor target, similar to that shown in Fig. I.5a. Note that experimental data show that similar to

poloidaly symmetric plasma detachment, divertor plasma detachment does also occur at plasma densities close to the density limit (e.g. see [25]).

Although some signatures of divertor plasma detachment were observed a long time ago (e.g. see Fig. 8 in [35]), intensive study of such regimes became one of the focal points of the magnetic fusion research only since 1990th (see the corresponding references in [25]). The interest to the detached divertor regime was driven by the need to reduce the power loading on the divertor targets in future tokamak-reactors, including ITER, to a tolerable level. The only way to do this is to re-radiate a significant fraction of the power, generated in the reactor, with impurity. However, the concept of strong impurity radiation from the core plasma has two issues. First, due to peculiarities of impurity cross-field transport in the core, strongly radiating, high-Z impurities (recall Fig. II.14) have a tendency of accumulation in the very core plasma, cooling it down and reducing the rate of fusion reactions. The radiation from low-Z impurities that are less prone to accumulation in the core plasma is rather weak, so for a sizeable effect, the concentration of the low-Z impurity must be high, with the corresponding dilution of the fusion D-T plasma and reduction of its performance. Secondly, a strong reduction of the heat flux from the core to the edge can prevent the transition to the improved confinement regime (H-mode), which may be needed for self-sustained burning of the fusion plasma. Therefore, it is widely accepted that it is necessary to increase power dissipation by impurity radiation in the divertor region as much as possible. There are two possible ways to do this: i) to increase the plasma/impurity density in the divertor region (recall that the density of the impurity radiation loss is proportional to the product of the electron and impurity densities) and ii) to increase the divertor volume by implementing so-called advanced divertor geometry (see Fig. I.6). It is very likely that in practice both ways will be combined.

However, an increase of the divertor plasma density will likely result in the increase of the plasma flux to the target and to the increase of the so-called "irreducible" power flux to the target, associated with the deposition of the internal energy of electron-ion pair – the ionization potential. Estimates made for ITER have shown that such "irreducible" power flux can exceed the tolerable power loading. As a result, in addition to the dissipation of plasma thermal power by impurity, it is also necessary to reduce the plasma particle flux to the target to a tolerable level. It seems that the detached divertor regime can meet both of these criteria (see Fig. I.6 and Fig. IX.10).

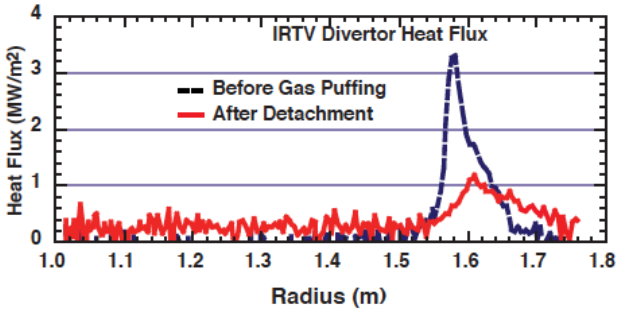

Fig. IX.10. Reduction of the power loading on the outer divertor target in DIII-D after the transition to the detached divertor regime. Reproduced with permission from [36], © IAEA 1999.

Shortly after initial experimental results on divertor plasma detachment became available, two main theoretical models, claiming their explanations, were put forward. The first one [37], [38] was relying on elastic (including charge-exchange) collisions of the plasma ions with the neutral gas in the divertor volume, which can switch plasma transport along the magnetic field lines from the fast, "ballistic" regime to the slow, "diffusive" one. As a result, "diffusive" plasma transport would cause a large plasma pressure drop between the upstream SOL region and the vicinity of the target (the so-called plasma "momentum removal") similar to that shown in [39]. This, according to [38],

can explain the reduction of the plasma flux to the target with increasing neutral gas density in the divertor and decreasing plasma temperature when the elastic ion-neutral collisions prevail over the electron impact ionization of neutrals. This model seems to be supported by experimental data from linear divertor simulators [40], [41], [42]. However, we will see later on that the data from linear divertor simulators, in this case, cannot be translated directly to the situation in a tokamak divertor.

The second model [43], [44] was based on energy and particle balance, including both the impurity radiation and the hydrogen "ionization" cost, as well as on the plasma recombination effect. In this model, the ion-neutral collisions *per se* do not result in the reduction of the plasma flux to the target. Nonetheless, they play an important role in the dissipation of the plasma momentum (via effective neutral viscosity) and thermal energy (via neutral heat conduction) at low temperatures when both the impurity and hydrogen radiation losses become inefficient.

Note that over the years, different models of the reduction of the plasma heat flux to the material surfaces, including both the ion-neutral collisions and plasma recombination were considered [45], [46], [47], [48].

2D numerical simulations of edge plasma transport performed with both UEDGE and SOLPS codes have shown that in agreement with [43], [44], the ion-neutral collisions alone cannot cause the reduction of the plasma flux to divertor targets [49], [50], [51], [52].

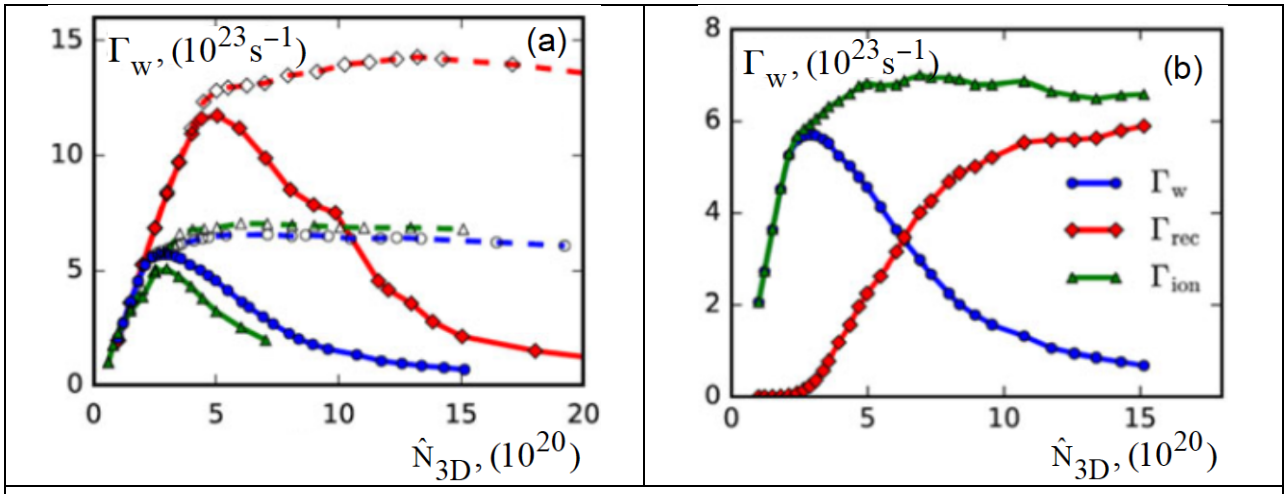

Fig. IX.11. (a) Γ_w as the function of $\hat{N}_{3D}$. Red lines: $Q_{SOL} = 8$ MW, $Q_{imp} = 0$ w/o recombination (dashed); $Q_{SOL} = 8$ MW, $Q_{imp} = 0$ with recombination (solid). Green lines: $Q_{SOL} = 8$ MW, $Q_{imp} = 4$ MW w/o recombination (dashed); $Q_{SOL} = 8$ MW, $Q_{imp} = 4$ MW with recombination (solid). Blue lines: $Q_{SOL} = 4$ MW, $Q_{imp} = 0$ w/o recombination (dashed); $Q_{SOL} = 4$ MW, $Q_{imp} = 0$ with recombination (solid). (b) Dependences of Γ_w, plasma ionization source, Γ_{ion}, and recombination sink, Γ_{rec}, on $\hat{N}_{3D}$ for $Q_{SOL} = 4$ MW, $Q_{imp} = 0$ with recombination turned on. Reproduced with permission from [51], © Cambridge University Press 2017.

As an example, in Fig. IX.11a the total plasma flux to the divertor targets and main chamber wall, Γ_w, is shown as the function of the total number of hydrogenic particles (including atoms and ions) in the computational domain, $\hat{N}_{3D}$, for different power input, Q_{SOL},

from the core plasma and the impurity radiation loss, Q_{imp}. $\hat{N}_{3D}$ can be considered a natural extension of the parameter N_{ft}^{tot} (which we used for the analysis of the SOL plasma parameters within a magnetic flux tube) to 2D modeling of edge plasma. The approach of the edge plasma simulations with fixed $\hat{N}_{3D}$ is called the "closed box" model, which, as demonstrated in [53], is a very good approximation for the high recycling regime where the plasma flux to the target exceeds by orders of magnitude both the puffing and pumping rates.

Note that at large $\hat{N}_{3D}$, plasma temperature in the vicinity of the targets falls below 1 eV and the neutral density becomes comparable to the plasma one, which, according to [38], is supposed to result in a reduction of the plasma flux. However, from Fig. IX.11a we see that Γ_w initially increases with increasing $\hat{N}_{3D}$ and then saturates unless plasma recombination is turned on. In addition, we notice that the saturation level of Γ_w at large $\hat{N}_{3D}$ is proportional to $Q_{SOL} - Q_{imp}$. From Fig. IX.11b, it follows that for a given Q_{SOL}, at large $\hat{N}_{3D}$ the plasma ionization source, Γ_{ion}, saturates, whereas the plasma recombination sink, Γ_{rec}, becomes almost equal to the ionization source, which causes the reduction of Γ_w.

All these observations have a simple physical explanation based on the model developed in [43], [44]. Following this model, we consider the energy and particle balance equations in the SOL for the high recycling conditions (ignoring hydrogen puffing and pumping):

$$Q_{SOL} = Q_{imp} + Q_H + Q_{CX} + \gamma T_w \Gamma_w, \tag{IX.12}$$

$$\Gamma_{ion} = \Gamma_w + \Gamma_{rec}, \tag{IX.13}$$

where Q_H is the power loss associated with hydrogen ionization; Q_{CX} describes the power delivered to the plasma-facing components by neutrals via the neutral-ion energy exchange (in dense divertor plasma this energy loss is related to neutral heat conductivity). The last term on the right-hand side of Eq. (IX.12) describes the transfer of the plasma thermal energy to the wall, and T_w is the averaged plasma temperature at the wall. By using the hydrogen ionization cost we have $Q_H = E_{ion}^H \Gamma_{ion}$. Since at high plasma density, both neutral heat and particle transport have diffusive nature, we have the estimate $Q_{CX} = \zeta_{\kappa/D} T_{ion} \Gamma_{ion}$, where T_{ion} is the temperature in the neutral ionization region and $\zeta_{\kappa/D} \approx 2.5$ [54] is the ratio of the neutral hydrogen heat and particle diffusivities. For the detached divertor regime, $T_{ion} \approx 3 \div 5\,\text{eV}$ and does not vary strongly since for lower temperature, the ionization rate constant drops sharply (see Fig. II.5).

For small T_w the last term in Eq. (IX.12) can be ignored and from Eq. (IX.12), (IX.13) we find

$$\Gamma_w = \frac{Q_{SOL} - Q_{imp}}{E_{ion}^{eff}} - \Gamma_{rec} \equiv \Gamma_{ion}^{max} - \Gamma_{rec}, \tag{IX.14}$$

where $E_{ion}^{eff} = E_{ion}^H + \zeta_{\kappa/D} T_{ion}$ is the effective ionization cost of neutral hydrogen accounting also for the energy loss associated with neutral heat conduction. We notice that the Γ_{ion}^{max} is limited by the power available for neutral ionization and this limit corresponds to the saturation level of

Γ_w in Fig. IX.11 for the case of no recombination. In agreement with the data shown in this figure, from Eq. (IX.14) we have $\Gamma_{ion}^{max} \propto Q_{SOL} - Q_{imp}$. Thus, from Eq. (IX.14) it follows that for low T_w, the reduction of Γ_w is only possible either by increasing the impurity radiation or by the plasma recombination processes (see Chapter II) or by both.

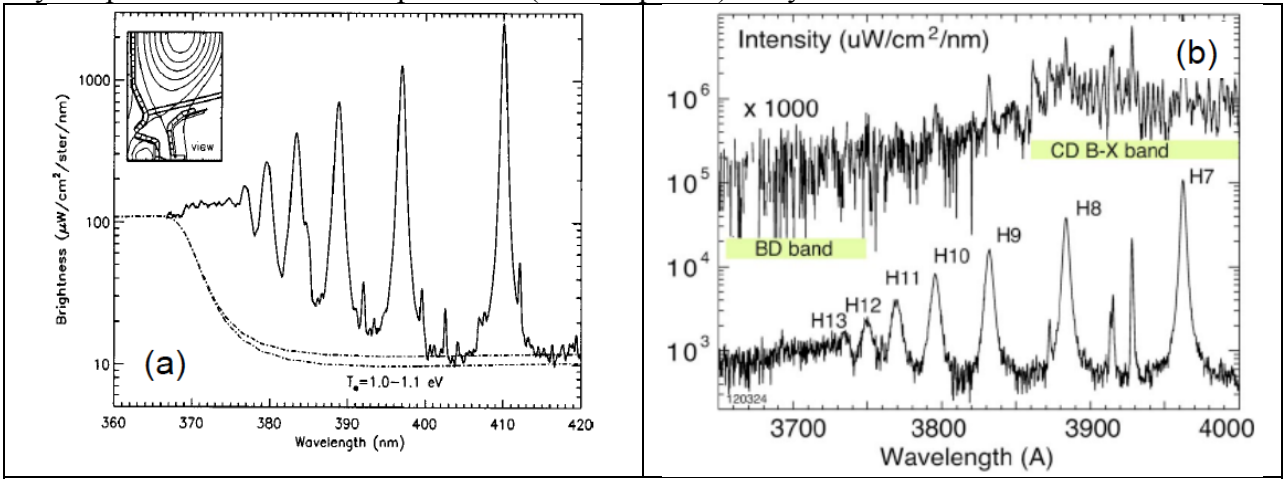

Fig. IX.12. Intensities of the Balmer series lines in (a, reproduced with permission from [55], © AIP Publishing 1998) detached recombining divertor plasma of C-Mod and (b, reproduced with permission from [56], AIP Publishing 2007) attached (upper curve) and detached recombining (lower curve) divertor plasma of NSTX tokamaks.

Available experimental data fully support the idea that the impurity radiation loss and plasma recombination are the main parameters determining the plasma flux to the targets at low T_w. Depending on the plasma conditions, either one can play the dominant role.

Clear signatures of volumetric plasma recombination were observed with spectroscopic diagnostics on many tokamaks [55], [57], [58], [59], [60], [61], [62]. For example, in Fig. IX.12 one can see the intensities of the Balmer series lines, which are typical for recombining plasmas (see also Fig. IX.3), from the C-Mod and NSTX tokamak divertors. Careful analysis of the plasma ionization source and the volumetric recombination sink in the C-Mod tokamak, performed in [63], has shown that Γ_{rec} can exceed 80% of Γ_{ion}. We notice that both electron-ion and molecular activated recombination (MAR), recall Chapter II, can contribute to the volumetric plasma particle loss. Recent experimental data from the TCV tokamak show that in the detached divertor regime, the contribution of MAR to the overall volumetric plasma recombination can reach ~40% [64].

Experimental data from both tokamaks [65], [66], [63], [67], [68] and stellarators [69], [70] show that in cold divertor plasma, the impurity radiation, in accordance with Eq. (IX.14), can also reduce the plasma flux to the targets.

An example demonstrating the impact of both plasma recombination and impurity radiation on the plasma flux to the divertor targets is shown in Fig. IX.13. As we see in the upper panel, just before the ICRF heating is on, plasma recombination is very close to the ionization source, which, however, is almost doubled when additional power for neutral ionization becomes available due to ICRF heating. On the lower panel, one sees that nitrogen puffing causes a strong reduction of plasma ionization source and, correspondingly reduction of the plasma flux to the targets, whereas the recombination sink remains small.

However, what to do with experimental data from linear divertor simulators [40], [41], [42], which seem to show that neutrals play an important role in the reduction of plasma flux to the target? We notice that in these experiments, the plasma was produced by the source situated in a separate chamber and only some portion of the generated plasma was flowing through an orifice into the working chamber. Therefore, the flux to the end target was significantly impacted by the neutral density in the working chamber. In addition, cross-field plasma transport in these experiments was relatively large and, for example, in [40] and [41] it was concluded that cross-field plasma transport is the main reason for the reduction of the plasma flux to the end target. As we see, the conditions of the plasma flow to the target in linear divertor simulators are very different from the tokamak ones, where all generated plasma particles are supposed either to flow to the plasma-facing components or to recombine volumetrically. Therefore, even though the experimental data obtained in linear divertor simulators on such issues as atomic physics and material erosion (see Chapter III) appear to be relevant for the edge plasma conditions in fusion devices (e.g. see [71], [72], [73] and the references therein), the results on plasma detachment cannot be transferred directly to the tokamak experiments.

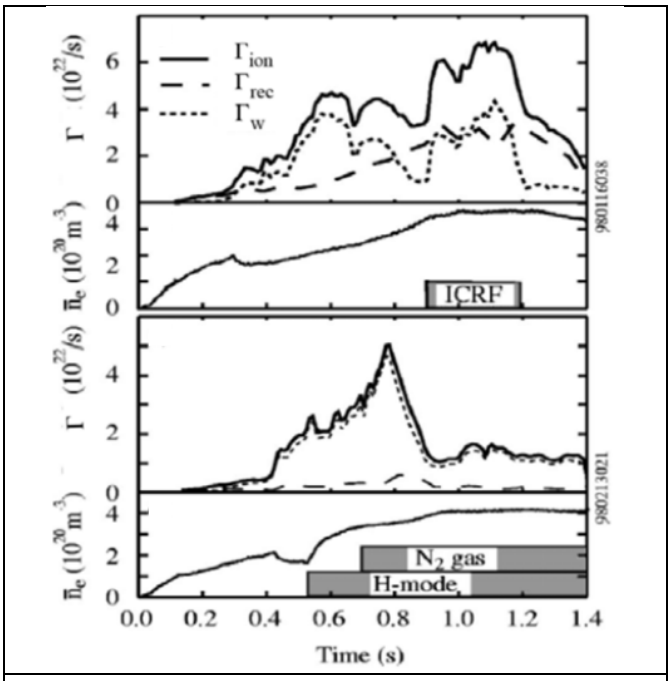

Fig. IX.13. Impact of the ion-cyclotron (ICRF) heating and nitrogen radiation loss on ionization source Γ_{ion} and plasma recombination sink Γ_{rec} in C-Mod tokamak. Reproduced with permission from [63], © AIP Publishing 1999.

Even though the simple physical picture, boiled down to Eq. (IX.14), for the plasma flux to the target in cold divertor plasma allows explaining the key experimental observations, it only describes the integral plasma flux to the plasma-facing components. However, from Fig. I.5b one sees that the divertor plasma detachment process does not happen uniformly over the entire divertor target. Instead, it starts from some particular flux tubes. Therefore, we need to find some local conditions for the onset of detachment, which we define as the beginning of the rollover of the specific plasma flux j_d. Following [74] we will use the same concept of the "closed box" for some particular magnetic flux tube, which we used for the analysis of the self-sustained tokamak divertor plasma oscillations. We notice that such an approach might be not directly suitable for the onset of divertor detachment in stellarators having a complex divertor magnetic geometry.

In the previous subsection, we found that for high recycling conditions, the plasma in the flux tube is sustained largely by the plasma recycling processes in the divertor region. However, the total pressure P_{ft}^{tot} within the flux tube, which can be supported by recycling, is limited by the power needed for hydrogen ionization and is determined by Eq. (IX.7), which can be expressed as follows

$$P_{ft}^{tot} \lesssim \left(P_{ft}^{tot}\right)_{max} = q_{recycl}\sqrt{\frac{M}{\gamma E_{ion}^{H}}}, \qquad \text{(IX.15)}$$

where $q_{recycl} = q_{ft} - q_{imp}$. In [74] it was shown that any further increase of P_{ft}^{tot} would result in a sharp reduction of the plasma temperature in the vicinity of the divertor targets, followed by a strong increase of plasma recombination and the reduction of the specific plasma flux to the target j_d. Thus we can consider the condition

$$\frac{P_{ft}^{tot}}{q_{recycl}} \approx \sqrt{\frac{M}{\gamma E_{ion}^{H}}} \approx 20\frac{N}{MW}, \qquad \text{(IX.16)}$$

as the criterion for the local onset of divertor plasma detachment at some particular flux tube [50] (we assume here deuterium plasma). We also notice that plasma recombination does not allow virtually any further increase of P_{ft}^{tot} beyond $\left(P_{ft}^{tot}\right)_{max}$ [74], [50], [52]. The reason for this is the strong increase of the plasma recombination rate, which effectively "dumps" any excessive plasma particles into the cold neutral gas cushion in the vicinity of the target and "freezes" P_{ft}^{tot} at the level determined by Eq. (IX.16). Recalling that the upstream plasma temperature is a weak function of q_{ft}, $T(L_{ft}) \propto (q_{ft}L_{ft})^{2/7}$, we find that the restriction for P_{ft}^{tot} effectively limits the accessible upstream plasma density and results in the so-called edge plasma density limit (e.g. see [75]).

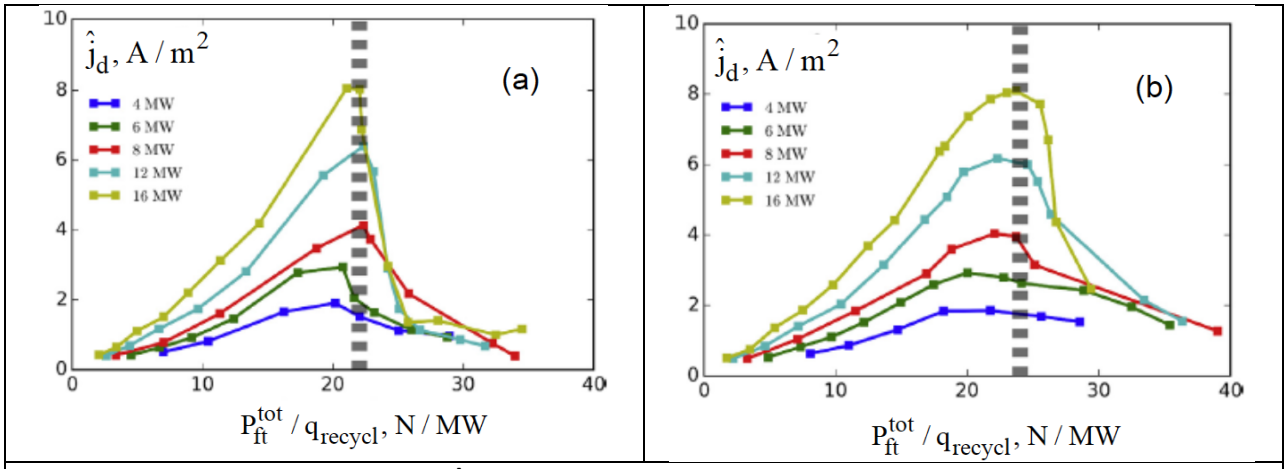

Fig. IX.14. The dependence of $\hat{j}_d$ close to the strike points in both the outer (a) and inner (b) divertors found from SOLPS simulations of a DIII-D-like tokamak as a function of $P_{ft}^{tot} / q_{recycl}$ for different Q_{SOL}. Reproduced with permission from [52], © Elsevier 2017.

These results on the onset of local divertor plasma detachment are supported by both comprehensive numerical simulations and experimental data. In Fig. IX.14 one can see the dependence of $\hat{j}_d$ (projection of j_d onto the target plane) close to the strike points in both the outer and inner divertors found from SOLPS simulations of a DIII-D-like tokamak (see [52] for

the details) as a function of $P_{ft}^{tot} / q_{recycl}$ for different Q_{SOL} in the closed box approximation. We notice that in agreement with Eq. (IX.16), the rollover of $\hat{j}_d$ occurs at the same value of the ratio $P_{ft}^{tot} / q_{recycl} \sim 20\ N/MW$ for both the inner and outer divertors independently of Q_{SOL}. A sharper rollover of $\hat{j}_d$ for larger Q_{SOL} is due to the higher divertor plasma density, which is more relevant for the consideration of isolated magnetic flux tube.

In addition, we notice that the impurity radiation loss is roughly proportional to the plasma density squared. Therefore the magnitude of $q_{recycl} = q_{ft} - q_{imp}$ decreases most strongly on the magnetic flux surfaces close to the separatrix, where the plasma density and, therefore, P_{ft}^{tot} are usually higher. As a result, the onset of divertor plasma detachment starts typically in the vicinity of the separatrix (recall Fig. I.5b), even though q_{ft} is higher in this region.

In Fig. IX.15 one can see the variation of P_{ft}^{tot} (in the same magnetic flux tube as in Fig. IX.14) as the function of $\hat{N}_{3D}$, found in the same simulations of a DIII-D-like tokamak. Whereas in the case with plasma recombination turned on P_{ft}^{tot} saturates with increasing $\hat{N}_{3D}$, with no recombination it increases continuously, which agrees with our theoretical model.

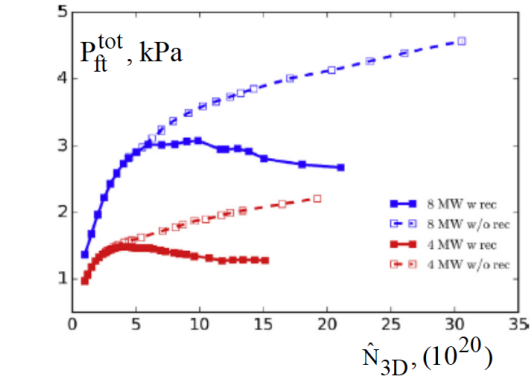

Fig. IX.15. P_{ft}^{tot} as the function of $\hat{N}_{3D}$ obtained from SOLPS simulation of a DIII-D-like tokamak. Reproduced with permission from [52], © Elsevier 2017.

The "freezing" of P_{ft}^{tot} with the onset of divertor plasma detachment results in important consequences for detachment of the inner and outer divertors. Due to the ballooning nature of cross-field plasma transport in a tokamak (recall Chapter VI), the heat flux into the outer divertor is usually larger than that coming into the inner one. However, the plasma pressure inside a given magnetic flux tube at the inner and outer sides of the torus in the vicinity of the separatrix is virtually the same. As a result, the ratio $P_{ft}^{tot} / q_{recycl}$ appears to be larger at the inner divertor and the latter starts to detach first. However, inner divertor detachment "freezes" P_{ft}^{tot} and does not allow the outer divertor to detach, until q_{recycl} at the outer divertor equilibrates with the inner one [76]. Such equilibration can happen due to E×B plasma flow or neutral influx through the private flux region from the inner to the outer divertor, which finally creates a backflow of the plasma in the outer SOL, thus reducing q_{recycl} [77], [76].

Recent careful spectroscopic measurements performed in [78] confirm that in the absence of the volumetric plasma recombination processes, the plasma flux on the divertor target is limited ($\Gamma_w \lesssim \Gamma_{ion}^{max}$) by the power flux into the recycling region as described by Eq. (IX.14), whereas the expression (IX.16) determines the rollover of the specific plasma flux to the target.

Even though the expressions (IX.14) and (IX.16) describe both the total plasma flux to the target and the local onset of detachment reasonably well, from the experimental and engineering points of view they are not very practical. Therefore, in [51], [76] the expression (IX.14) was recast in terms of the neutral hydrogen, P_H, and impurity, P_{imp}, pressures in the divertor.

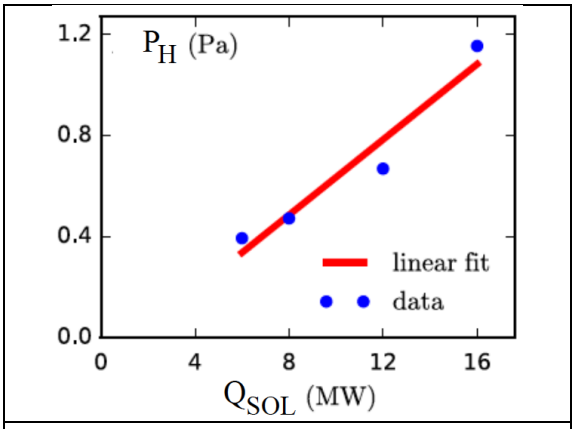

Fig. IX.16. Neutral hydrogen pressure in divertor corresponding to the rollover of Γ_w as the function of Q_{SOL}, found from numerical simulation of DIII-D-like plasma. Reproduced with permission from [76], © AIP Publishing 2017.

In addition, following [79] we introduce an effective "ionization cost" for the impurity, E_{ion}^{imp}, which describes the energy radiated by an impurity ion during the time from ionization to complete recombination in the volume or neutralization on a material surface. So the impurity radiation loss in Eq. (IX.14) can be written as $Q_{imp} = E_{ion}^{imp}\Gamma_{imp}$, where Γ_{imp} is the impurity influx into the divertor plasma. Then, taking into account that both the neutral impurity and hydrogen fluxes into the divertor plasma are proportional to their pressures and that divertor plasma detachment starts when Q_{SOL} is dissipated by the energy loss associated with the impurity and hydrogen "ionization costs", we find the following condition for the onset of plasma detachment

$$Q_{crit} \equiv C_{det}\left\{P_H + (E_{ion}^{imp}/E_{ion}^{H})\sqrt{M_H/M_{imp}}P_{imp}\right\} \gtrsim Q_{SOL}, \qquad \text{(IX.17)}$$

where C_{det} is the normalization constant which depends on both the magnetic topology and the geometrical configuration of the divertor, M_H and M_{imp} are the masses of, correspondingly, hydrogen and impurity particles.

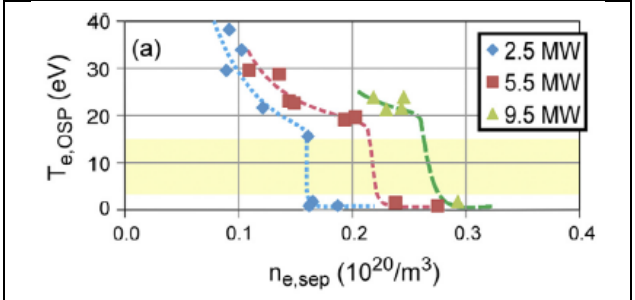

Fig. IX.17. Bifurcation-like transition to detached outer divertor in the DIII-D tokamak with increasing separatrix plasma density. Reproduced with permission from [81], © Elsevier 2015.

From [79], we find the estimate $E_{ion}^{imp} \sim 3\,\text{keV}$ for the low-Z impurities (although this value can depend on the magnetic topology and the geometrical configuration of the divertor). Then, taking $E_{ion}^{H} \sim 40\,\text{eV}$ and $M_H/M_{imp} \sim 0.1$, from Eq. (IX.17) we find $Q_{crit} \propto P_H + 25 \times P_{imp}$, which is in the same ballpark with the recent experimental data from ASDEX Upgrade (see Eq. (1) from [80]). Numerical simulations from [76] also support the expression (IX.17), see Fig. IX.16. The available experimental data demonstrate that both gradual evolution and bifurcation-like transition to the detached divertor regime are possible.

In Fig. IX.17 one can see a bifurcation-like change of the electron temperature at the outer strike point as the separatrix plasma density in DIII-D increases [81]. On the contrary, in JET with the ITER-like wall (ILW), the gradual evolution of the plasma flux on both the inner and outer divertor targets along with the increase of the core plasma density was observed [82], Fig. IX.18.

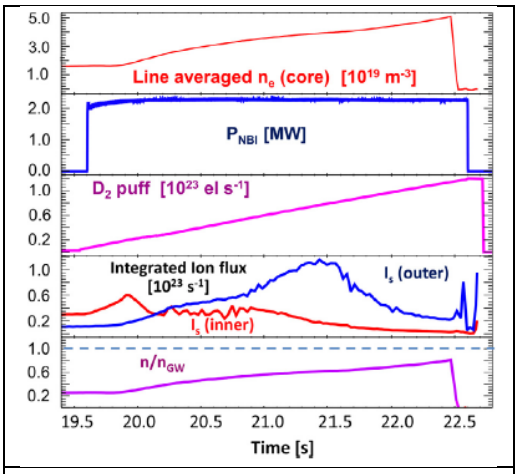

Fig. IX.18. Evolution of the plasma parameters in JET-ILW. Reproduced with permission from [82], © Elsevier 2013.

The bifurcation-like transition into the detached state can be explained by different mechanisms. For example: by the N-shape dependence $T_d(N_{ft}^{tot})$, shown schematically in Fig. IX.8, by impurity radiation [83], [84], by hydrogen outgassing from the targets [85], by and impact of divertor plasma detachment on anomalous cross-field plasma transport [51], and by the effects of the drifts [86], [87] see Fig. IX.19. However, we notice that the simplified models, which are often used for analytic and semi-analytic estimates, do not allow for many important effects of both plasma and impurity dynamics. Therefore their conclusions should be taken with caution and need to be verified with more comprehensive numerical simulations. In particular, 2D numerical simulations of detachment in a DIII-D-like plasma show that a gradual increase of the impurity (neon) content results in a smooth reduction of the plasma flux to the target and propagation of the detachment front towards the X-point [51]. The reason for this is the progressive accumulation of the impurity in the cold, virtually non-radiative divertor region that expands gradually. This effect plays the role of negative feedback and prevents the development of thermal bifurcation. We also notice that even the simulations with advanced 2D edge plasma transport codes often show only qualitative agreement with the experimental data

For example, although the experimental data and the results of 2D numerical simulations (see Fig. IX.19) of outer divertor detachment in the DIII-D tokamak, which emphasize the role of the E×B drifts, agree qualitatively, the numbers still do not match each other.

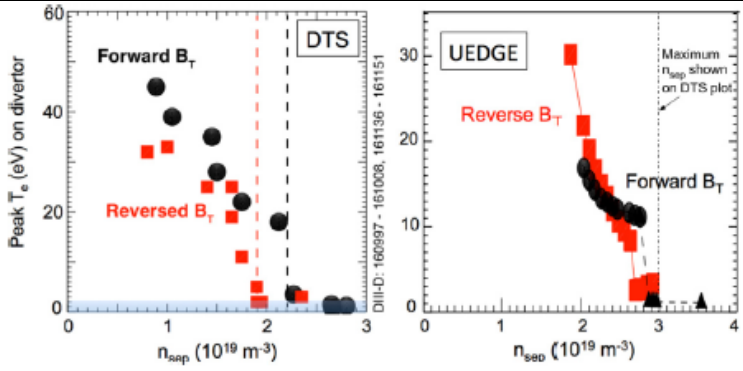

Fig. IX.19. Peak electron temperature on the outer divertor target, found from (left) divertor Thomson scattering and (right) 2D UEDGE simulations. Reproduced with permission from [86], © Elsevier 2017.

Two important knobs that can facilitate divertor plasma detachment are the magnetic configuration and the geometry of plasma-facing components (e.g. see Fig. I.6). Whereas a magnetic configuration with multiple X-points can decrease the power coming to particular strike points (e.g. see the snowflake and X-point target divertors in Fig. I.6), the geometry of the plasma-facing components, which "confine" the neutrals in the vicinity of the divertor targets, can

reduce the plasma ionization source Γ_{ion} and enhance the plasma energy sink caused by neutral heat conduction in low temperature (~1 eV) plasma, where the radiation processes become inefficient.

The reduction of Γ_{ion} in a carefully "baffled" divertor can be seen from the following. We recall that for the case where all neutrals are ionized in the recycling region, Γ_{ion} is bounded by the expression $\Gamma_{ion} \tilde{<} Q_{recycl} / E^{H}_{ion}$. However, when neutral baffling is poor, some of the neutrals are bypassing the main recycling region and can go beyond the impurity radiation region, see Fig. IX.20. As a result, the potential ionization source related to these neutrals is now limited by $Q_{SOL} > Q_{recycl}$, which can greatly complicate the rollover of Γ_w. Experimental data also demonstrate that the so-called "closed", well baffled, divertors have a low threshold of the upstream plasma density for detachment (e.g. see [88]).

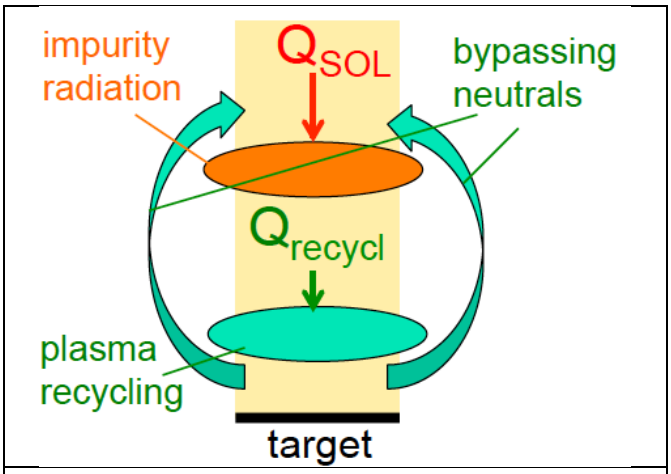

Fig. IX.20. Neutrals bypassing impurity radiation region can face large power available for neutral ionization

Conclusions for Chapter IX.

As we have discussed, the edge plasma exhibits different nonlinear phenomena resulting in the formation of macroscopic strongly radiative and recombining structures (e.g. MARFE, detached divertor), nonlinear oscillations and bifurcations. In many cases, atomic physics effects, including impurity and hydrogen radiation, drive some of these phenomena. Others are associated with the interplay of atomic physics effects and cross-field plasma transport (including drifts and anomalous transport) as well as with plasma interactions with the materials of plasma-facing components. Some of these phenomena (e.g. divertor plasma detachment) can be affected by magnetic configuration and geometry of plasma-facing components.

Whereas some of these phenomena can be very beneficial for the performance of future fusion reactors (e.g. divertor plasma detachment can drastically reduce power and particle loading on divertor targets), others (e.g. MARFE formation close to separatrix) can result in the degradation of core plasma confinement and the reduction of overall reactor performance.

Even though large progress was made in the understanding of the physics of these nonlinear phenomena (e.g. divertor plasma detachment) still much more work is needed for better assessment of edge plasma behavior in future reactors.

References for Chapter IX

[1] B. Lipschultz, B. LaBombard, E. S. Marmar, M. M. Pickrell, J. L. Terry, R. Watterson, S. M. Wolfe, "Marfe: an edge plasma phenomenon", Nucl. Fusion **24** (1984) 977-988.

[2] J. Neuhauser, W. Schneider, R. Wunderlich, "Thermal instabilities and poloidal asymmetries in the tokamak edge plasma", Nucl. Fusion **26** (1986) 1679-1692.

[3] J. F. Drake, "MARFES: Radiative condensation in tokamak edge plasma", Phys. Fluids 30 (1987) 2429-2433.

[4] B. Meerson, "Nonlinear dynamics of radiative condensations in optically thin plasmas", Rev. Mod. Phys. **68** (1996) 215-257.

[5] C. Mazzotta, G. Spizzo, G. Pucella, E. Giovannozzi, O. Tudisco, G. Apruzzese, W. Bin, B. Esposito, the FTU team, " Dynamic and frequency behavior of the MARFE instability in FTU", Nucl. Mater. Energy **12** (2017) 808-812.

[6] A. V. Chankin "on the poloidal localization and stability of multi faceted asymmetric radiation from the edge (MARFE)", Phys. Plasmas **11** (2004) 1484-1482.

[7] D. R. Baker, R. T. Snider, M. Nagami, "Observations of cold high-density plasma near Doublet III limiter", Nucl. Fusion **22** (1982) 807-811.

[8] F. P. Boody, C. E. Bush, S. S. Medley, H. K. Park, and J. F. Schivell, "Phenomenology of MERFE in TFTR", J. Nucl. Mater. **145-147** (1987) 196-200.

[9] B. Lipschultz, "Review of MARFE phenomena in tokamaks", J. Nucl. Mater. **145-147** (1987) 15-25.

[10] W. M. Stacey, "A Survey of Thermal Instabilities in Tokamak Plasmas: Theory, Comparison with Experiment, and Predictions for Future Devices" Fusion Sci. Techn. **52** (2006) 29-67.

[11] M. Asif and the Hefei Tokamak-7 team. "The phenomenon of multifaceted asymmetric radiation from the edge with new graphite limiters in Hefei Tokamak-7" Plasma Dev. Oper. **15** (2007) 27-32.

[12] R. Dachicourt, P. Monier-Garbet, C. Gil, R. Guirlet, P. Tamain, O. Meyer, P. Devinck, B. Pégorié, F. Clairet, J. Bucalossi, Y. Corre, J. L. Ségui, "Bifurcation to a stable MARFE in Tore Supra", J. Nucl. Mater. **438** (2013) S334-337.

[13] B. J. Peterson, Yuhong Xu, S. Sudo, T. Tokuzawa, K. Tanaka, M. Osakabe, S. Morita, M. Goto, S. Sakakibara, J. Miyazawa, K. Kawahata, N. Ohyabu, H. Yamada, O. Kaneko, A. Komori, and LHD Experimental Group, "Multifaceted asymmetric radiation from the edge-like asymmetric radiative collapse of density limited plasmas in the Large Helical Device", Phys. Plasmas **8** (2001) 3861-3864.

[14] U. Wenzel, C. Biedermann, G. Kocsis, T. Szepesi, B.D. Blackwell, S. Klose, J. Knauer, M. Krychowiak, L. Stephey, O. Schmitz, J. Harris, R. König, T.S. Pedersen and the W7-X Team, "Observation of Marfes in the Wendelstein 7-X stellarator with inboard limiters", Nucl. Fusion **58** (2018) 096025.

[15] M. Greenwald, "Density limit in toroidal plasmas", Plasma Phys. Control. Fusion **44** (2002) R27-R80.

[16] P. C. de Vries, J. Rapp, F. C. Schüller, and M. Z. Tokar', "Influence of Recycling on the Density Limit in TEXTOR-94 ", Phys. Rev. Lett. **80** (1998) 3519-3522.

[17] B. Lipschultz, J. L. Terry, C. Boswell, A. Hubbard, B. LaBombard, and D. A. Pappas, "Ultrahigh Densities and Volume Recombination inside the Separatrix of the Alcator C-Mod Tokamak", Phys. Rev. Lett. **81** (1998) 1007-1010.

[18] A. N. Simakov and S. I. Krasheninnikov, "Ionization-recombination instability and multifaceted asymmetric radiation from the edge in magnetic fusion devices", Phys. Plasmas **7** (2000) 850-856.
[19] D. Kh. Morozov and J. J. E. Herrera, "Slow Thermal Waves in Impurity Seeded Radiative Plasmas", Phys. Rev. Lett. **76** (1996) 760-763.
[20] R. D. Smirnov, A. S. Kukushkin S. I. Krasheninnikov, A. Y. Pigarov and T. D. Rognlien "Impurity-induced divertor plasma oscillations", Phys. Plasmas **23** (2016) 012503.
[21] J. D. Strachan, F. P. Boody, C. E. Bush, S. A. Cohen, B. Grek, L. Grisham, F. C. Jobes, D. W. Johnson, D. K. Mansfield, S. S. Medley, W. Morris, H. K. Park, J. F. Schivell, G. Taylor, K. L. Wong, S. Yoshikawa, M. C. Zarnstorff, and S. J. Zweben, "Experimental results from detached plasmas in TFTR", J. Nucl. Mater. **145-147** (1987) 186-190.
[22] F. Alladio, R. Bartiromo, B. Casali, P. Buratti, F. De Marco, M. De Pretis, R. Giannella, M. Grolli, L. Pieroni, A. Tanga, A. Tuccillo and O. Tudisso, "The regime of enhanced particle recycling in high density tokamak discharges in the Frascati Torus", Phys. Lett. A **90** (1982) 405-409.
[23] G. M. McCracken, J. allen, K. Axon, R. Barnsley, S. J. Fielding, D. H. J. Goodall, N. Hawkes, J. Hugill, P. C. Johnson, G. F. Mathews and C. S. Pitcher, "A study of detached plasma in the DITE tokamak", J. Nucl. Mater. **145-147** (1987) 181-185.
[24] U. Samm, P. Bogen, H. A. Classen, H. Gerhauser, H. Hartwig, E. Hintz, Y. T. Lie, A. Pospieszczyk, D. Rusbüld and B. Schweer, "Influence of Impurity Radiation Losses on Plasma Edge Properties in TEXTOR," J. Nucl. Mater. **176-177** (1990) 273-277.
[25] G. F. Matthews, "Plasma detachment from divertor targets and limiters", J. Nucl. Mater. **220-222** (1995) 104-116.
[26] U. Wenzel, P. Bachmann, A. Carlson, M. Laux, B. Napiontek, M. Weinlich, "Relaxation oscillations in the divertor of the ASDEX Upgrade tokamak", Nucl. Fusion **37** (1997) 1343-1347.
[27] A. Loarte, R. D. Monk, A. S. Kukushkin, E. Righi, D. J. Campbell, G. D. Conway, and C. F. Maggi, "Self-Sustained Divertor Plasma Oscillations in the JET Tokamak", Phys. Rev. Lett. **83** (1999) 3657-3660.
[28] M. Kobayashi, S. Masuzaki, I. Yamada, N. Tamura, Y. Feng, K. Sato, M. Goto, Y. Narushima, T. Akiyama, J. Miyazawa, M. Shoji, S. Morita, B. J. Peterson, H. Funaba, N. Ohyabu, K. Narihara, T. Morisaki, H. Yamada, A. Komori, LHD Experimental Group, and D. Reiter, "Detachment stabilization with n/m=1/1 resonant magnetic perturbation field applied to the stochastic magnetic boundary of the Large Helical Device", Phys. Plasmas **17** (2002) 056111.
[29] S. I. Krasheninnikov, A. S. Kukushkin, V. I. Pistunovich, V. A. Pozharov, "Poloidal-divertor Operating Regimes with Natural Oscillations", Sov. Tech. Phys. Lett. **11** (1985) 440-442.
[30] S. I. Krasheninnikov, A. S. Kukushkin, V. I. Pistunovich, V. A. Pozharov, "Self-sustained oscillations in the divertor plasma", Nucl. Fusion **27** (1987) 1805-1816.
[31] K. Lackner, R. Chodura, M. Kaufman, J. Neuhauser, K. G. Rauh, & W. Schneider, "Control of particle and energy transport across the boundary of a tokamak plasma", Plasma Phys. Control. Fusion **26** (1984) 105-115.
[32] K. Borras, "Disruptive tokamak density limit as scrape-off layer/divertor phenomenon", Nucl. Fusion **31** (1991) 1035-1051.

[33] A. S. Kukushkin, S. I. Krasheninnikov, "Bifurcations and oscillations in divertor plasma", Plasma Phys. Control. Fusion **61** (2019) 074001.
[34] D. Coster, "Characterization of oscillations observed in reduced physics SOLPS simulations", Nucl. Mater. Energy **12** (2017) 666-674.
[35] Y. Shimomura, M. Kaufman, K. Lackner, & H. Murman, "Characteristics of the divertor plasma in neutral-beam-heated ASDEX discharges", Nucl. Fusion **23** (1983) 869-879.
[36] ITER Physics Basis, Chapter 4: Power and particle control. Nucl. Fusion **39** (1999) 2391-2469.
[37] P.-H. Rebut, D. Boucher, D. J. Gambier, B. E. Keen, and M. L. Watkins "The ITER challenge", Fusion Eng. and Design **22** (1993) 7-18.
[38] P. C. Stangeby, "Can detached divertor plasmas be explained as self-sustained gas targets?", Nucl. Fusion **33** (1993) 1695-1705.
[39] S. A. Self & H. N. Ewald, "Static theory of a discharge column at intermediate pressures", Phys. Fluids **9** (1966) 2486-2492.
[40] W. L. Hsu, M. Yamada, & P. J. Barret, "Experimental simulation of the gaseous tokamak divertor", Phys. Rev. Lett. 49 (1982) 1001-1004.
[41] G. Fiksel, M. Kishinevsky & N. Hershkowitz, "Experimental simulation of a gaseous plasma collector", Phys. Fluids B **2** (1990) 837-841.
[42] L. Schmitz, R. Lehmer, G. Chevalier, G. Tynan, P. Chia, R. Doerner, & R. W. Conn, "Experimental simulation of the gaseous divertor concept in PISCES-A", J. Nucl. Mater. **176-177** (1990) 522-527.
[43] S. I. Krasheninnikov, "Divertor plasma detachment: present status of understanding", Contrib. Plasma Phys. **36** (1996) 293-303.
[44] S. I. Krasheninnikov, A. Yu. Pigarov, D. A. Knoll, B. Labombard, B. Lipschultz, D. J. Sigmar, T. K. Soboleva, J. L. Terry, & F. Wising, " Plasma recombination and molecular effects in tokamak divertors and divertor simulators", Phys. Plasmas **4** (1997)1638-1646.
[45] I. E. Tamm and A. D. Sakharov, 1961, in *Proceedings of the Second International Conference on the Peaceful Uses of Nuclear Energy* (ed. by M. A. Leontovich, Oxford, Pergamon 1961), vol. 1, pp. 1-47.
[46] B. Lehnert, "Screening of a high-density plasma from neutral gas penetration", Nucl. Fusion **8** (1968) 173-181.
[47] F. H. Tenney, "Divertor operation in the princeton reference design model tokamak reactor", J. Nucl. Mater. **53** (1974) 43-47.
[48] S. I. Krasheninnikov & A. Yu. Pigarov, "Super-dense regimes of the divertor in tokamak reactor", Nucl. Fusion Supplement **3** (1987) 387-394.
[49] F. Wising, D. A. Knoll, S. I. Krasheninnikov, T. D. Rognlien, & D. J. Sigmar, "Simulation of detachment in ITER-geometry using the UEDGE code and fluid neutral model" Contrib. Plasma Phys. **36** (1996) 309–313.
[50] S. I., Krasheninnikov, A. S. Kukushkin, & A. A. Pshenov, "Divertor plasma detachment", Phys. Plasmas **23** (2016) 055602.
[51] S. I. Krasheninnikov and A. S. Kukushkin, "Physics of ultimate detachment of a tokamak divertor plasma", J. Plasma Phys. **83** (2017) 155830501.
[52] A. A. Pshenov, A. S. Kukushkin, S. I., Krasheninnikov, "Energy balance in plasma detachment", Nucl. Mater. Energy **12** (2017) 948-952.
[53] A. Yu. Pigarov, "Detached divertor with acceptable separatrix Z_{eff}", Phys. Plasmas **24** (2017) 102521.

[54] P. Helander, S. I. Krasheninnikov, & P. J. Catto, "Fluid equations for a partially ionized plasma", Phys. Plasmas **1** (1994) 3174–3180.
[55] J. L. Terry, B. Lipschultz, A. Yu. Pigarov, S. I. Krasheninnikov, B. Labombard, D. Lumma, H. Ohkawa, D. Pappas, & M. Umansky, "Volume recombination and opacity in Alcator C-Mod divertor plasmas", Phys. Plasmas **5** (1998) 1759–1766.
[56] V. A. Soukhanovskii, D. W. Johnson, R. Kaita, and A. L. Roquemore," Electron density measurements in the National Spherical Torus Experiment detached divertor region using Stark broadening of deuterium infrared Paschen emission lines", Review of Scientific Instruments **77** (2006) 10F127
[57] R. C. Isler, G. R. Mckee, N. H. Brooks, W. P. West, M. E. Fenstermacher, & R. D. Wood, "Signatures of deuterium recombination in the DIII-D divertor", Phys. Plasmas **4** (1997) 2989-2996.
[58] G. M. Mccracken, M. F. Stamp, R. D. Monk, A. G. Meigs, J. Lingertat, R. Prentice, A. Starling, R. J. Smith, & A. Tabasso, "Evidence for volume recombination in JET detached divertor plasmas", Nucl. Fusion **38** (1998) 619–629.
[59] U. Wenzel, K. Behringer, A. Carlson, J. Gafert, B. Napiontek, & A. Thoma, "Volume recombination in divertor I of ASDEX Upgrade", Nucl. Fusion **39** (1999) 873–882.
[60] A. Tabasso, J. Dowling, J.-W. Ahn, G. Cunningham, A. Kirk, G. Mcardle, M. Price, & The MAST TEAM "Analysis of the progress to detachment in the divertor of the MAST tokamak", J. Nucl. Mater. **313–316** (2003) 936-940.
[61] V. A. Soukhanovskii, R. Maingi, D. A. Gates, J. E. Menard, S. F. Paul, R. Raman, A. L. Roquemore, R. E. Bell, C. E. Bush, R. Kaita, H. W. Kugel, B. P. LeBlanc, D. Mueller and the NSTX Team, "Divertor heat flux mitigation in high-performance H-mode discharges in the National Spherical Torus Experiment", Nucl. Fusion **49** (2009) 095025.
[62] J. R. Harrison, W. A. J. Vijvers, C. Theiler, B. P. Duval, S. Elmore, B. Labit, S. H. M. van Limpt, S. W. Lisgo, C. K, Tsui, H. Reimerdes, U. Sheikh, K. H. S. Verhaegh, M. Wischmeier, the MST1 and TCV teams. "Detachment evolution on the TCV tokamak", Nucl. Mater. Energy **12** (2017) 1071-1076.
[63] B. Lipschultz, J. L. Terry, C. Boswell, J. A. Goetz, A. E. Hubbard, S. I. Krasheninnikov, B. LaBombard, D. A. Pappas, C. S. Pitcher, F. Wising, and S. Wukitch, "The role of particle sinks and sources in Alcator C-Mod detached divertor discharges", Phys. Plasmas **6** (1999) 1907-1916.
[64] B. Lipschultz, private communication, 2019.
[65] R. D. Monk, A. Loarte, A. Chankin, S. Clement, S. J. Davis, J. K. Ehrenberg, G. Y. Guo, J. Lingertat, G. F. Matthews, M. F. Stamp, P. C. Stangeby, "Interpretation of ion flux and electron temperature profiles at the JET divertor target during high recycling and detached discharges", J. Nucl. Mater. **241-243** (1997) 396-401.
[66] J. A. Goetz, B. LaBombard, B. Lipschultz, C. S. Pitcher, J. L. Terry, C. Boswell, S. Gangadhara, D. Pappas, J. Weaver, B. Welch, R. L. Boivin, P. Bonoli, C. Fiore, R. Granetz, M. Greenwald, A. Hubbard, I. Hutchinson, J. Irby, E. Marmar, D. Mossessian, M. Porkolab, J. Rice, W. L. Rowan, G. Schilling, J. Snipes, Y. Takase, S. Wolfe, and S. Wukitch, "High confinement dissipative divertor operation on Alcator C-Mod", Phys. Plasmas **6** (1999) 1899-1906.
[67] K. Verhaegh, B. Lipschultz, B. P. Duval, J. R. Harrison, H. Reimerdes, C. Theiler, B. Labit, R. Maurizio, C. Marini, F. Nespoli, U. Sheikh, C. K. Tsui, N. Vianello, W. A. J. Vijvers, the TCV team and the EUROfusion MST1 team, "Spectroscopic investigation of divertor detachment in TCV", Nucl. Mater. Energy **12** (2017) 1112-1117.

[68] B. Lomanowski, M. Carr, A. Field, M. Groth, A. E. Jaervinen, C. Lowry, A. G. Meigs, S. Menmuir, M. O'Mullane, M. L. Reinke, C. K. Stavrou, S. Weisen, JET contributors, "Spectroscopic investigation of N and Ne seeded induced detachment in JET ITER-like wall L-modes combining experiment and EDGE2D modeling", Nucl. Mater. Energy **20** (2019) 100676.
[69] J. Miyazawa, S. Masuzaki, H. Yamada, R. Sakamoto, B. J. Peterson, M. Shoji, N. Ohyabu, A. Komori, O. Motojima, LHD Experimental Group, P. Grigull, Y. Feng, K. McCormick, F. Sardei, Yu. Igitkhanov & W7-As Team, "Detachment Phenomena in LHD Compared to W7-AS", Fusion Sci. Techn. **50** (2006) 192-200.
[68] D. Zhang, R. König, Y. Feng, R. Burhenn, S. Brezinsek, M. Jakubowski, B. Buttenschön, H. Niemann, A. Pavone, M. Krychowiak, S. Kwak, J. Svensson, Y. Gao, T. S. Pedersen, A. Alonso, J. Baldzuhn, C. D. Beidler, C. Biedermann, S. Bozhenkov, K. J. Brunner, H. Damm, M. Hirsch, L. Giannone, P. Drewelow, F. Effenberg, G. Fuchert, K. C. Hammond, U. Höfel, C. Killer, J. Knauer, H. P. Laqua, R. Laube, N. Pablant, E. Pasch, F. Penzel, K. Rahbarnia, F. Reimold, H. Thomsen, V. Winters, F. Wagner, T. Klinger, and W7-X team, "First Observation of a Stable Highly Dissipative Divertor Plasma Regime on the Wendelstein 7-X Stellarator", Phys. Rev. Lett. **123** (2019) 025002.
[71] N. Ohno, N. Ezumi, S. Takamura, S. I. Krasheninnikov, & A. Yu. Pigarov, "Experimental evidence of molecular activated recombination in detached recombining plasmas", Phys. Rev. Lett. **81** (1998) 818-821.
[72] A. Okamoto, S. Kado, K. Sawada, Y. Kuwahara, Y. Iida, S. Tanaka, "Contribution of hydrogen molecular assisted recombination processes to population of hydrogen atom in divertor simulator MAP-II" J. Nucl. Mater. **363-365** (2007) 395-399.
[73] K. Nojiri, M. Sakamoto, N. Ezumi, A. Terakado, T. Iijima, S. Togo, T. Yokodo, Y. Kinoshita, T. Mikami, T. Yoshimoto, S. Yamashita, J. Kohugara, M. Yoshikawa, Y. Nakashima, "Effects of gas puff and pump on plasma detachment associated with molecular activated recombination in GAMMA 10/PDX", Nucl. Mater. Energy **20** (2019) 100691.
[74] S. I. Krasheninnikov, M. Rensink, T. D. Rognlien, A. S. Kukushkin, J. A, Goetz, B. LaBombard, B. Lipschultz, J. L. Terry, & M. Umansky, "Stability of the detachment front in a tokamak divertor", J. Nucl. Mater. **266-269** (1999) 251-257.
[75] K. Borrass, D. Coster, Reiter, & R. Schneider, "Study of recombining gas targets", J. Nucl. Mater. **241-243** (1997) 250-254.
[76] A. A. Pshenov, A. S. Kukushkin, S. I., Krasheninnikov, "On detachment asymmetry and stability", Phys. Plasmas **24** (2017) 072508.
[77] A. Kukushkin and H. Pacher, "Divertor modelling and extrapolation to reactor conditions", Plasma Phys. Control. Fusion **44** (2002) 931-943.
[78] K. Verhaegh, B. Lipschultz, B. P. Duval, O. Février, A. Fil1, C. Theiler, M. Wensing, C. Bowman, D. S. Gahle, J.R. Harrison, B. Labit, C. Marini, R. Maurizio, H. de Oliveira, H. Reimerdes, U. Sheikh, C. K. Tsui, N. Vianello, W. A. J. Vijvers, the TCV team and the EUROfusion MST1 team, "An improved understanding of the roles of atomic processes and power balance in divertor target ion current loss during detachment", To appear in Nucl. Fusion 2020.
[79] M. Z. Tokar And F. A. Kelly, "The role of plasma–wall interactions in thermal instabilities at the tokamak edge", Phys. Plasmas **10** (2003) 4378-4386.
[80] A. Kallenbach, M. Bernert, M. Beurskens, L. Casali, M. Dunne, T. Eich, L. Giannone, A. Herrmann, M. Maraschek, S. Potzel, F. Reimold, V. Rohde, J. Schweinzer, E. Viezzer, M.

Wischmeier and the ASDEX Upgrade Team "Partial detachment of high power discharges in ASDEX Upgrade" Nucl. Fusion **55** (2015) 053026.
[81] A. G. McLean, A. W. Leonard, M. A. Makowski, M. Groth, S. L. Allen, J. A. Boedo, B. D. Bray, A. R. Briesemeister, T. N. Carlstrom, D. Eldon, M. E. Fenstermacher, D. N. Hill, C. J. Lasnier, C. Liu, T. H. Osborne, T. W. Petrie, V. A. Soukhanovskii, P. C. Stangeby, C. Tsui, E. A. Unterberg, J. G. Watkins, "Electron pressure balance in the SOL through the transition to detachment", J. Nucl. Mater. **463** (2015) 533-536.
[82] A. Huber, S. Brezinsek, M. Groth, P.C. de Vries, V. Riccardo, G. van Rooij, G. Sergienko, G. Arnoux, A. Boboc, P. Bilkova, G. Calabro, M. Clever, J.W. Coenen, M.N.A. Beurskens, T. Eich, S. Jachmich, M. Lehnen, E. Lerche, S. Marsen, G.F. Matthews, K. McCormick, A.G. Meigs, Ph. Mertens, V. Philipps, J. Rapp, U. Samm, M. Stamp, M. Wischmeier, S. Wiesen, JET-EFDA contributors. "Impact of the ITER-like wall on divertor detachment and on the density limit in the JET tokamak", J. Nucl. Mater. **438** (2013) S139-S147.
[83] I. H. Hutchinson, "Thermal front analysis of detached divertor and MARFE", Nucl. Fusion **34** (1994) 1337-1348.
[84] S. I. Krasheninnikov, "Two-dimensional effects in plasma radiation fronts and radiation front jumps in tokamak divertor plasmas", Phys. Plasmas 4 (1997) 3741-3743.
[85] T. Nakano, N. Asakura, H. Takenaga, H. Kubo, Y. Miura, K. Shimizu, S. Konoshima, K. Masaki, S. Higashijima, and The JT-60TEAM "Impact of wall saturation on particle control in long and high-power-heated discharges in JT-60U" Nucl. Fusion **46** (2006) 626-634.
[86] T. D. Rognlien, A. G. McLean, M. E. Fenstermacher, M. Groth, A. E. Jaervinen, I. Joseph, C. J. Lasnier, W. Meyer, A. Moser, G. D. Porter, M. V. Umansky, "Comparison of 2D simulations of detached divertor plasmas with divertor Thomson measurements in the DIII-D tokamak", Nucl. Mater. Energy **12** (2017) 44-59.
[87] A. E. Jaervinen, S. L. Allen, D. Eldon, M. E. Fenstermacher, M. Groth, D. N. Hill, A.W. Leonard, A. G. McLean, G. D. Porter, T. D. Rognlien, C. M. Samuell, and H. Q. Wang, "E×B flux driven detachment bifurcation in the DIII-D Tokamak", Phys. Rev. Lett. **121** (2018) 075001.
[88] B. Lipschultz, B. Labombard, J. L. Terry, C. Boswell, and I. Hutchinson, "Divertor physics research on Alcator C-Mod", Fusion Sci. Techn. **51** (2007) 369–389.